Received: 2 February 2024 | Accepted: 8 March 2024

DOI: 10.1002/pc.28326

RESEARCH ARTICLE

Polymer COMPOSITES WILEY

$SiO_2@Al_2O_3$ binary filler: A chance for enhancing the heat transport in rubber composites for tire applications

Lorenzo Mirizzi[1] | **Andreia Amighini Alerhush**[1] | **Roberto Nisticò**[1] | **Mery Malandrino**[2] | **Sandra Diré**[3,4] | **Emanuela Callone**[3,4] | **Giulia Fredi**[3] | **Andrea Dorigato**[3] | **Luca Giannini**[5] | **Silvia Guerra**[5] | **Silvia Mostoni**[1] | **Barbara Di Credico**[1] | **Roberto Scotti**[1,6] | **Massimiliano D'Arienzo**[1]

[1]Department of Materials Science, INSTM, University of Milano-Bicocca, Milano, Italy

[2]Department of Chemistry, NIS Interdepartmental Centre, University of Torino, Turin, Italy

[3]Department of Industrial Engineering, University of Trento, Trento, Italy

[4]"Klaus Müller" Magnetic Resonance Lab, DII, University of Trento, Trento, Italy

[5]Pirelli Tyre SpA, Milano, Italy

[6]Institute for Photonics and Nanotechnologies-CNR, Povo (TN), Italy

Correspondence
Roberto Nisticò and Massimiliano D'Arienzo, Department of Materials Science, INSTM, University of Milano-Bicocca, Via R. Cozzi 55, Milano 20125, Italy.
Email: roberto.nistico@unimib.it and massimiliano.darienzo@unimib.it

Funding information
CORIMAV

Abstract

The present study reports on the development of a new binary filler system for rubber composites, $SiO_2@Al_2O_3$, where Al_2O_3 sheets are grown onto SiO_2 nanoparticles aggregates by a sustainable water-based soft-chemistry approach. The aim is to synergistically integrate the intrinsic thermal conductivity properties of Al_2O_3 with the peculiar reinforcement ability of SiO_2 in an easy one-pot solution, which has been exploited to prepare polybutadiene (PB) model composites by a simple solvent casting technique. More in detail, the binary filler was used as-prepared or suitably surface functionalized with 3-(Trimethoxysilyl) propylmethacrylate (TMSPM). The filler compatibilization and interplay with the polymeric matrix have been inspected by solid state NMR in conjunction with scanning electron microscopy. These investigations highlighted that the presence of alumina in the binary filler does not undermine the capability of silica in generating polymer chains stiffening and indicated a significant effect of the silanization in providing better filler networking and interaction with the PB host ensuring, in principle, an enhanced thermal transport. Accordingly, thermal conductivity measurements revealed that $SiO_2@Al_2O_3$ introduction in PB induces a remarkable upgrade of the heat transfer, which becomes much more relevant upon surface modification with TMSPM. These results appear encouraging, paving the possibility of applying $SiO_2@Al_2O_3$ model system to more complex case studies, where both improved thermal conductivity and enhanced reinforcement are required, such as tires tread formulations.

Highlights

- A new $SiO_2@Al_2O_3$ binary filler system was proposed following a soft-chemistry approach.
- The binary filler was functionalized to enhance its compatibilization.
- Fillers were dispersed in polybutadiene by a simple solvent casting technique.
- Thermal conductivity measurements revealed a remarkable upgrade of the heat transfer ability.

KEYWORDS

alumina, inorganic fillers, nanocomposites, polymer composites, surface functionalization, thermal conductivity

1 | INTRODUCTION

Polymers and polymer composites are materials largely used in several aspects of our daily life and large-scale industrial applications (e.g., automotive and aeronautics, (opto)electronics, photonics, biomedical devices, packaging industry, ESD protective systems, and so on) due to their intrinsic properties, namely: easy manufacturing and processing, design freedom, lightweight, excellent water/corrosion resistance, relatively low cost, etc.[1–10] Unfortunately, these outstanding properties are coupled with an intrinsic low thermal conductivity (k) deriving from the polymeric matrix, typically 0.1–0.5 W m^{-1} K^{-1} at room temperature (RT).[11,12] Hence, heat dissipation remains one of the major problems affecting the thermal stability of these materials, which limits their in-service life and performances, especially in the case of systems working under dynamic service conditions, such as rubber composites for tires.[13,14] In fact, during their utilization under dynamic conditions, tires are subjected to internal friction phenomena involving filler-filler and filler-matrix mechanical interactions causing heat buildup might favor undesired degradation phenomena.[15,16]

To overcome the above issues, the current approaches proposed by the scientific literature pursue the addition in the rubber formulations of thermal conductive filler, which, in principle, generate a continuous filler network in the polymer matrix, granting the thermal transport.[17]

These strategies do not easily fit with the safety, operative (e.g., stability at high velocity, wet grips, rolling resistance, etc.), and environmental requirements that tires must satisfy,[18] which are remarkably connected to their mechanical properties and, in turn, to the rubber matrix characteristics and filler morphological/surface features.

In this context, several reports dealing with tires application primarily proposed the use of carbonaceous anisotropic filler such as 1D carbon nanotubes,[19–21] 2D graphene (oxide) and graphite,[22–24] and carbon (nano)fibers[21] due to their intrinsic high k values (100–4000 W m^{-1} K^{-1}).[25] Even if extremely promising, these systems present several drawbacks, among which the filler alignment along the in-plane direction as well as the high filler volume fraction in order to attain an efficient heat dissipation, resulting in difficult composite processability and costs increment.[25]

Despite their generally lower thermal conductivity, ceramics represent a valid alternative to carbon-based filler. Hexagonal boron nitride (h-BN, ca. 400–2000 W m^{-1} K^{-1}),[26] alumina (Al_2O_3, ca. 30–40 W m^{-1} K^{-1}),[17] aluminum nitride (AlN, ca. 210–320 W m^{-1} K^{-1}),[27] silicon carbide (SiC, ca. 100 W m^{-1} K^{-1}),[28] and zinc oxide (ZnO, ca. 60 W m^{-1} K^{-1})[29] were generally employed in composites, thanks to their intrinsic k values and to the ability of successfully dissipate local heat buildup by forming thermal conductive pathways across the polymeric matrix.

However, as these systems own a different chemistry respect to the rubber formulations containing silica and silicate as fillers,[30–33] their utilization for this specific purpose is still limited, mainly due to the high filler loading required, their costs and the concerns related to their surface functionalization, which should ensure remarkable interfacial adhesion among the filler and macromolecular chains, avoiding the occurrence of phonon scattering and interfacial thermal resistance.[34]

In this complex scenario, our recent study,[25] outlined the option to exploit Al_2O_3 nanoparticles (NPs) and polyhedral silsesquioxane (POSS) units, to fabricate an unconventional Al_2O_3@POSS hybrid filler, merging the abilities of both systems, namely the networking capability of POSS units with the enhanced thermal conductivity of alumina, aiming at obtaining rubber nanocomposites with enhanced thermal and mechanical features.

Few other examples of Al_2O_3 utilization in rubber composites for tires are present in the literature pointing out the critical role played by particle size and anisotropy.[16,34] In particular, it was highlighted that large and anisotropic alumina particles (e.g., micrometer sized) favor the thermal dissipation but negatively affect the mechanical properties, whereas small particles (nanometer sized) display beneficial effects on the mechanical properties, but do not significantly affect the thermal conductivity.[16,34]

Bearing in mind all these considerations and in view of tire application, an interesting option would be combining alumina with common silica NPs utilized in industrial formulation. In this regard, Vaisakh et al.,[35] described the inclusion of a silica/alumina mixed system in a thermoset epoxy matrix and its beneficial effect both in terms of thermal conductivity and mechanical properties, suggesting a potential synergistic action between the two components.

Although focused on epoxy composites, these results inspired us to investigate the possibility of introducing in elastomers commonly exploited in tire tread formulations, alumina particles in conjunction with SiO_2 NPs.

In light of the extensively described concerns related to the alumina surface compatibilization, we decided to convey this filler in the rubber matrix not just simply mixing with silica, but through the development of a new binary filler system, $SiO_2@Al_2O_3$ where alumina sheets are grown onto commercially available SiO_2 NPs aggregates. The aim is to combine the thermal conductivity features imparted by the alumina without sacrificing the reinforcement ability of silica component.

Upon the comprehensive assessment of the composition, structure and morphology, the binary filler was used, as prepared or suitably surface functionalized with 3-(Trimethoxysilyl)propylmethacrylate (TMSPM), to prepare cis-polybutadiene (PB) model composites by a simple solution blending technique.

The filler compatibilization and interaction with the polymeric matrix were evaluated in detail, in conjunction with the morphology and the thermal conductivity of the composites. The obtained performances were also compared to those of a composite obtained by simply mixing $SiO_2@Al_2O_3$ and TMSPM in the polymer matrix.

Results evidenced that the introduction of the $SiO_2@Al_2O_3$ in PB induces a remarkable upgrade of the heat transport capability compared to the neat polymer matrix. Moreover, the surface modification of the binary filler with TMSPM emphasizes this effect, suggesting a role of the surface functionalization in providing high *k* and mitigating the filler-rubber interfacial thermal resistance.

2 | EXPERIMENTAL

2.1 | Chemicals

Inorganic salts and compounds: Commercial silica (SiO_2, Zeosil® 1165, Solvay), alumina (Al_2O_3, gamma-phase, 99%, Thermo Scientific Chemicals), aluminum nitrate nonahydrate ($Al(NO_3)_3{\cdot}9H_2O$, 98%, Fluka Analytical), aluminum sulfate octadecahydrate ($Al(SO_4)_3{\cdot}18H_2O$, 97 + %, Acros Organics), and urea ($CO(NH_2)_2$, 99.5%, Sigma-Aldrich). Potassium bromide (KBr, 99+%, FT-IR grade, Aldrich) is maintained dried at ca. 80°C. *Acid solutions*: Nitric acid (65%, Sigma-Aldrich), hydrofluoric acid (48%, Sigma-Aldrich), ammonium hydrogen difluoride ($(NH_4)HF_2$, 98.7%, VWR Chemicals), boric acid (H_3BO_3, Supelco). *Solvents*: Toluene (99.9%, Aldrich), ethanol (absolute, Honeywell). *Polymers*: cis-Polybutadiene (PB, average M_w 200,000-300,000, Aldrich). *Other reactants*: 3-(Trimethoxysilyl)propylmethacrylate (TMSPM, 98%, Sigma-Aldrich), azobisisobutyronitrile (AIBN, 98 wt.%, Sigma-Aldrich). Milli-Q water with a resistivity of 18.2 MΩ cm is used.

2.2 | Synthesis of the $SiO_2@Al_2O_3$ binary filler

$SiO_2@Al_2O_3$ binary filler was synthesized modifying a procedure reported in the literature.[36] In detail, commercial silica (ca. 4.00 g) is dispersed in 500 mL of deionized water by sonication for 15 min (sol. 1). Then, urea (ca. 15.00 g), aluminum nitrate (ca. 8.04 g), aluminum sulfate (ca. 1.12 g) are dissolved inside a 3 L-round bottom flask in 2 L of deionized water by magnetic stirring (sol. 2). The amount of precursors is selected in order to obtain a $SiO_2@Al_2O_3$ binary filler with composition 70 wt.% SiO_2 and 30 wt.% Al_2O_3. After dissolution of the alumina precursors, the silica suspension (sol. 1) is added to the precursor aqueous solution (sol. 2). The resulting reaction mixture is maintained under magnetic stirring and heated up to 120°C (isothermal step for ca. 3 h) until it becomes turbid and pH reaches a value of *approx.* 7.0 (neutral). After cooling to RT, the suspension is vacuum filtered, and the obtained solid washed with deionized water, and oven dried at 80°C overnight. Finally, the crystallization of the alumina phase is performed by thermally treating the solid in a muffle furnace at 1100°C for 1 h (heating rate 5°C min^{-1}) under air atmosphere.

2.3 | Surface functionalization of the $SiO_2@Al_2O_3$ binary filler

$SiO_2@Al_2O_3$ binary filler was functionalized with TMSPM following a modified procedure present in the literature.[37] In detail, $SiO_2@Al_2O_3$ binary filler (ca. 1.0 g) is dispersed inside a round bottom flask in 24 mL of toluene by sonication for 15 min. Subsequently, TMSPM (ca. 0.3 g) is added dropwise to the mixture. The suspension is maintained under magnetic stirring and kept at 120°C for ca. 12 h. After cooling to RT, the suspension is centrifuged (9000 rpm) for 15 min, washing the solid with toluene (2×) and ethanol (1×), in order to eliminate traces of non-reacted TMSPM. Then, the obtained solid ($SiO_2@Al_2O_3$-TMSPM) is oven dried at 80°C overnight. The same strategy has been adopted to functionalize SiO_2 NPs (i.e., SiO_2-TMSPM sample).

2.4 | Preparation of the PB-based nanocomposites

Bare SiO_2, SiO_2-TMSPM, $SiO_2@Al_2O_3$ and $SiO_2@Al_2O_3$-TMSPM binary filler were incorporated into PB via solvent-casting to produce composites, following a modified procedure present in the literature.[25] In detail, PB (ca. 2.0 g) is dissolved inside a round bottom flask in

15 mL of anhydrous toluene for ca. 12 h (overnight, without stirring) in order to obtain the complete swelling of the polymer. Subsequently, the mixture is magnetically stirred and heated up to 65°C. Separately, a suspension containing the desired amount of selected filler in 10 mL of toluene is prepared by sonication for 30 min. Afterwards, the prepared filler suspension and AIBN (ca. 0.04 g, 2 wt.% respect to the PB) are added simultaneously to the hot PB solution, and the reaction mixture is stirred and refluxed under nitrogen atmosphere, at 65°C for 6 h. The obtained solutions are solvent cast by depositing the hot polymer/filler system in Teflon Petri dishes. To remove volatiles, the samples are maintained overnight at 65°C under an aspiration hood and then heated at 70°C for 2.5–3.0 h in a vacuum. The composite samples (ca. 700 μm thick) are stored under N_2 atmosphere until all the characterizations are performed, to avoid any possible contamination. Hereafter, the different PB-based composites are labeled PB/XY, where X refers to the filler nominal content (expressed in wt.%, namely: 10, 20, 30), while Y refers to the filler type, namely: SiO_2, SiO_2-TMSPM, $SiO_2@Al_2O_3$, and $SiO_2@Al_2O_3$-TMSPM. For the sake of comparison, a reference composite containing a physical mixture of $SiO_2@Al_2O_3$ and TMSPM (i.e., with the TMSPM not linked at the surface of the filler) with a total nominal filler content of 20 wt.% was also prepared. The ratio between $SiO_2@Al_2O_3$ and TMSPM was estimated from the quantification of the amount of TMSPM linked at the surface of the $SiO_2@Al_2O_3$-TMSPM filler by means of TGA (vide infra). This reference sample is labeled as PB/20$SiO_2@Al_2O_3$ + TMSPM. Furthermore, as an additional reference material, bare PB was prepared by following the same experimental procedure used for the preparation of the PB-based composites, this time without adding any filler. This reference sample is labeled as PB.

2.5 | Characterizations

XRD patterns were collected with a Rigaku Miniflex 600 diffractometer, with a Cu source working at the following conditions 40 kV and 15 mA, investigating the 10–70°2θ range, applying a 0.02° step size, and 1 degree per minute of angular velocity. Instrumental PDXL-2 software is used for recognizing the crystal phases (ICDD PDF# 29-0063).

Multinuclear solid-state NMR spectra of both filler and composites were recorded with a Bruker Avance 400WB spectrometer equipped with a CPMAS probe: ^{27}Al at 104.67 MHz, π/2 Hahn-echo pulse length 2.2 μs, recycle delay 3 s, n° scans 1 k. ^{29}Si at 79.48 MHz, single pulse sequence π/4 pulse length 3.9 μs, recycle delay 300 s, scans 1 k, with contact time of 5 ms and recycle delay for cross polarization of 10 s. ^{13}C at 100.48 MHz, decoupling length 5.9 μs, n° scans 5 k, with contact time of 2 ms and recycle delay of 3 s. ^{1}H at 400.13 MHz, single pulse sequence π/2 pulse 6.6 μs, recycle delay 5 s, n° scans 16. Samples were filled in zirconia rotors (4 mm) spun at either 8 or 11 kHz, under air flow. External secondary references selected were: 1 M $Al(NO_3)_3$ aqueous solution, Q_8M_8 and adamantane $C_{10}H_{16}$. Structural units involving Si are labeled following the NMR notation: T^n indicates R-SiO_3 Si-units, Q^n indicates SiO_4 Si-units, with the apex *n* indicating the number of oxo-bridges. Lineshape analysis has been performed by using the Bruker TopSpin 3.6 instrumental software, with 95% as acceptable confidence level.

Relaxation studies were performed using a spin-lock pulse sequence with a variable spinlock pulse in a 0.5–500 ms range (with a 20 kHz frequency field for the spin-lock field B_1) for the evaluation of $T_{1\rho(H)}$[25,38] and CPMG sequence setting the echo time in the 8–2000 ms range for the evaluation of T_2.[25,39] In these experiments the proton spectrum intensity M (magnetization) as a function of t (a variable interval, which depends on the specific experiment, during which M relaxes until the original equilibrium state is reached) is recorded in order to evaluate different specific ranges of molecular dynamics. For all of them, the trend of M(t) is generally an exponential decay with a characteristic time constant. The two experiments were tested in order to extract the time constants T_2 and $T_{1\rho(H)}$, that are correlated to different frequency ranges, and consequently their values are influenced by molecular motions on different time scales. The calculated values are commonly obtained by fitting the experimental curve ([40] and references therein).

SEM measurements were performed on a Zeiss Gemini 500 microscope with both secondary electrons and Bruker Quantax detectors, the latter one for the EDS/WDS (Energy Dispersive/Wave Dispersive) elemental analysis. The reliability of the morphological analysis is guaranteed by the large number of micrographs collected (at least 10) for every filler and composites, sampling different regions of all sample. In the case of nanocomposites, both surface view and cross-section (by orthogonally cutting the nanocomposites with a cutter) view are sampled.

TEM measurements on filler were performed on a Jeol JEM-2100Plus working at 200 kV (with a 0.24 nm point-to-point resolution). Fillers were suspended in an ethanol environment, depositing a single drop of every suspension onto a carbon film supported on a 3 mm metallic Cu grid for performing the TEM analysis.

The Al concentration is determined by inductively coupled plasma—optical emission spectroscopy (ICP-OES—Optima 7000 DV Perkin Elmer) equipped with a Cross Flow nebulizer, a Scott spray chamber and an

Echelle monochromator. The wavelength was 396.153 nm (Al). Every single concentration value was measured considering the mean value of n° 3 instrumental measurements. The acid dissolution procedure selected is performed in a microwave oven (Milestone Ethos ONE). Different sample aliquots (n° 3) were dissolved following a two-step procedure. In the first step, the acid mixture is made by 9 mL HNO_3, 4 mL HF, and 1.0 g $(NH_4)HF_2$, whereas in the second step the acid mixture is made by only 1.4 g H_3BO_3. The resulting solutions were diluted to 25 mL with high-pure water. For the sake of comparison, three different physical mixtures of silica: alumina in wt. ratio 90:10, 80:20, and 70:30 were prepared and measured.

FTIR spectra of filler were recorded in transmission mode on KBr pellets by means of a Jasco-4100 spectrophotometer, equipped with DTGS detector, applying the Blackman-Harris apodization function (4 cm^{-1} resolution, 4000–500 cm^{-1} spectral range, 128 scans). Samples are analyzed after background subtraction performed on a bare KBr pellet. ATR-FTIR spectra of composites are recorded on a Thermo Fisher Nicolet iS20 FTIR spectrometer (4 cm^{-1} resolution, 4000–500 cm^{-1} spectral region, 32 scans).

TGA thermograms were collected by means of a Mettler Toledo TGA/DSC1 STARe System, at a constant air flow (50 cm^3 min^{-1}), following the thermal programs: Filler characterization: (i) pre-heating at 150°C (rate: 5°C min^{-1}, time: 15 min) to remove residual humidity/solvent, (ii) heating ramp from 150 to 1000°C (rate: 10°C min^{-1}), (iii) isothermal step at 1000°C (time: 5 min). The TGA curves are used to determine the quantity of hydroxyl functionalities present at the surface of the bare $SiO_2@Al_2O_3$ binary filler, and the weight loss due to the organic functionalizing agent (TMSPM).

Composites characterization: heating ramp from 30 to 1000°C (rate: 10°C min^{-1}), under air atmosphere. The TGA curves were used to determine the amount of inorganic filler in the composites.

LFA measurements were performed on a LFA 467 analyzer (Netzsch Holding Gmbh). Measurements are carried out under RT on discoidal specimens (diameter: 12.7 mm), die cut and coated with a graphitic layer spraying both sides. For each composition at least n° 2 specimens are tested, performing at least N° 5 pulses on every single specimen. Data are processed with the dedicated Proteus® software applying a transparent model with linear baseline and numerical pulse correction. This procedure allowed measuring the thermal diffusivity (α), thus the thermal conductivity value (k) at 25°C was calculated using the following (Equation 1):

$$k = \alpha \cdot \rho \cdot C_p \quad (1)$$

where ρ is the density (measured at at 23.0°C with a pycnometer) and C_p is the specific heat calculated from a differential scanning calorimetry (DSC) run in accordance to the standard ASTM E1269-11.

3 | RESULTS AND DISCUSSION

3.1 | Characterization of the $SiO_2@Al_2O_3$ binary filler

The structural characterization of the $SiO_2@Al_2O_3$ binary filler was performed by means of powders XRD analysis and reported in Figure 1A. The diffraction pattern of the binary filler shows the typical broad signal at 2θ ca. 22° due to amorphous silica.[41] Additionally, two weak signals at 2θ = 45.5°, and 66.7° are attributed to the (400) and (440) crystalline planes of the γ-phase of Al_2O_3.[42,43] Interestingly, the diffractogram of the $SiO_2@Al_2O_3$ binary filler does not show any peaks associated to the thermally induced transformation of commercial amorphous silica into its crystalline form, thus suggesting that the growth of alumina phase prevents the silica crystallization. The morphology of the $SiO_2@Al_2O_3$ binary filler was investigated by TEM (Figure 1B–D), whereas the EDS microanalysis (Figure 1E) was evaluated to qualitatively assign a specific morphology to a given phase. In particular, Figure 1B highlights the presence of aggregates of SiO_2 spherical NPs with diameter of *ca*. 30–40 nm surrounded or partially covered by sheet-like nanostructures with length ranging between 50 and 150 nm. Higher resolution TEM image (Figure 1C) reveals the crystallinity of the sheet-like nanostructure at the surface of silica aggregates. Finally, the EDS microanalysis performed for site 1 and site 2 in Figure 1D confirms the different chemical nature of the binary filler components, with a prevalence of Si and O signals in the case of spherical particles (Figure 1E, site 1), while the dominant occurrence of Al and O in the case of nanosheets (Figure 1E, site 2), thus suggesting the successful growth of alumina on the surface of silica aggregates. Furthermore, the alumina morphology is in accordance with the sheet-like structure of bohemite, initially formed during the colloidal synthesis (i.e., before the thermal treatment), and it is maintained even after alumina crystallization.[44] The relatively large size of these crystalline nanostructures along with their peculiar anisotropy should in principle guarantee a better continuity of the heat transport and, in turn, enhanced thermal conductivity when enclosed in polymer composites.[17,35]

To further study the interfacial interaction between silica and alumina phases forming the $SiO_2@Al_2O_3$

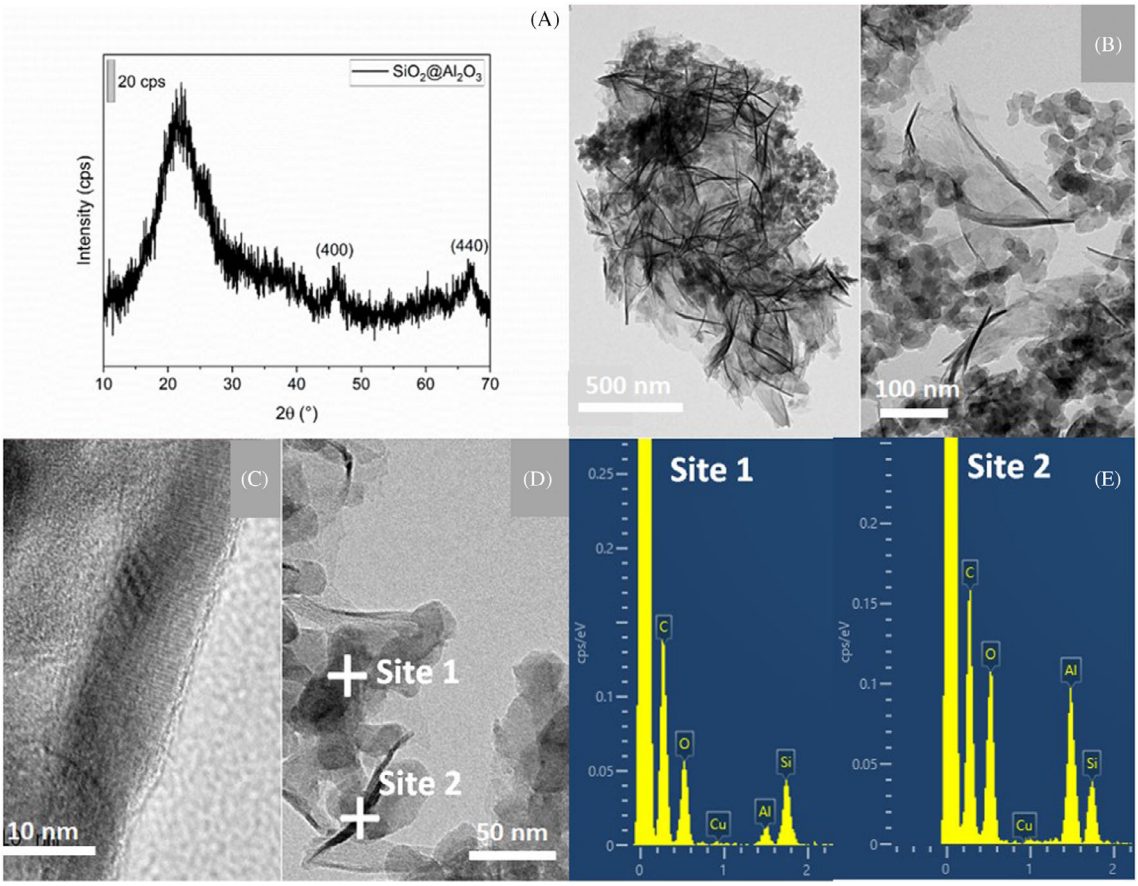

FIGURE 1 Structural and morphological characterization of the $SiO_2@Al_2O_3$ binary filler. (Panel A) XRD pattern of the $SiO_2@Al_2O_3$ with marked signals due to γ-Al_2O_3. (Panel B) TEM images of $SiO_2@Al_2O_3$. (Panel C) High resolution TEM images of $SiO_2@Al_2O_3$. (Panel D) TEM images of the $SiO_2@Al_2O_3$ binary filler with marked sites sampled during the EDS microanalysis. (Panel E) EDS microanalyses for site 1 (amorphous silica) and site 2 (γ-Al_2O_3).

binary filler, ^{27}Al and ^{29}Si MAS NMR spectra were acquired on bare silica, bare alumina, and $SiO_2@Al_2O_3$ binary filler (Figure 2).

The ^{29}Si MAS NMR spectra of commercial silica nanoparticles and $SiO_2@Al_2O_3$ binary filler show the resonance of the Q units (Figure 2, left). For the amorphous silica particles the resonance is composed by the typical Q^2, Q^3 and Q^4 components centered at −90.0 (1.8%), −100.3 (23.6%) and −110.5 (74.6%) ppm, respectively. The $SiO_2@Al_2O_3$ binary filler spectrum presents a different Q line-shape, in particular the amount of non-completely condensed units (i.e., Q^2 and Q^3 signals) is slightly reduced, by the thermal treatment, but also probably by the grafting of the alumina nanosheets on the silica surface, which induces the formation of Al-O-Si bonds (namely Q^4(1Al) units). This is proved by the increase of Q^4 units from 75 up to 92% at the expenses of Q^3 and Q^2.[45,46] Thus, the ^{29}Si MAS NMR analysis suggests successful surface functionalization of the silica, thus forming a silica-alumina binary system. Both ^{27}Al spectra of commercial gamma-alumina nanoparticles and $SiO_2@Al_2O_3$ binary filler are characterized by the presence of two resonances centered at about 7.7 and 59 ppm, due to octahedral and tetrahedral Al sites, respectively (Figure 2, right).[45] With respect to commercial alumina, the $SiO_2@Al_2O_3$ sample presents a higher amount of tetrahedral Al, whose resonance appears upfield shifted and slightly modified in shape, indicating a variation of the chemical environment of the Al sites.

In accordance with the literature,[47,48] it is possible to separate this resonance into two different components centred at 68 and 50 ppm. They are attributable to Al-O-Al (65%) and Al-O-Si (35%) bonds, respectively.[47,48] The presence of the Al-O-Si component is an index of interaction with silica particles. Moreover, the increase of the intensity of the tetrahedral Al sites indicates that the Al-O-Si bonds force the Al atoms and their Al nearest neighbors to adopt a silica-like coordination mode, thus coherently proving the growth of alumina onto silica particles.

The Al content in our $SiO_2@Al_2O_3$ binary filler was quantified by means of ICP-OES. Numerical values (Table S1) confirmed that the content in alumina is

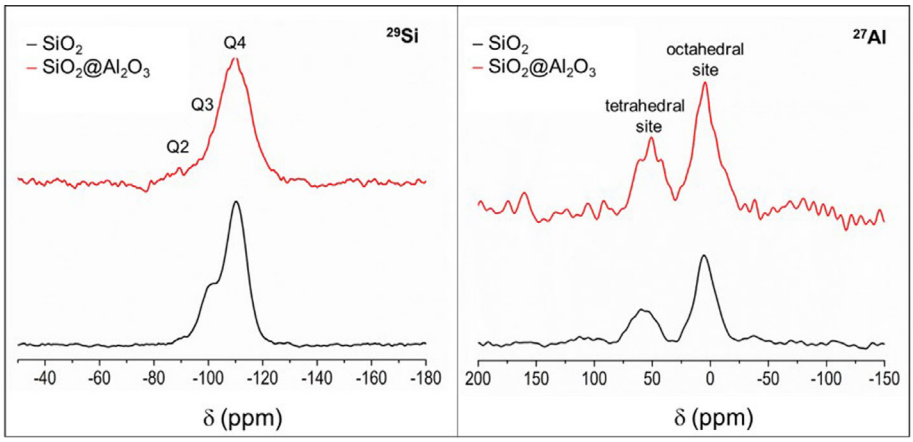

FIGURE 2 Left-side: ^{29}Si MAS NMR spectra of commercial silica (black line), and $SiO_2@Al_2O_3$ (red line). Right-side: ^{27}Al Hahn-echo NMR spectra of commercial reference alumina (black line), and $SiO_2@Al_2O_3$ (red line).

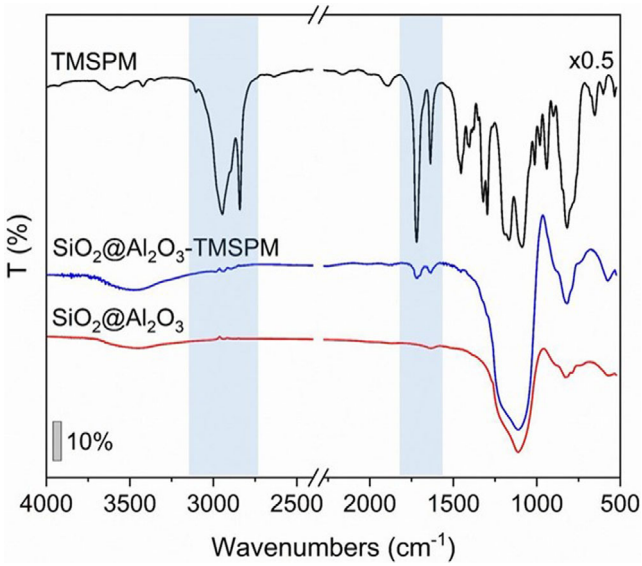

FIGURE 3 FTIR spectra in transmission mode of bare $SiO_2@Al_2O_3$ binary filler (red line), bare TMSPM (black line), and $SiO_2@Al_2O_3$-TMSPM (blue line).

approx. 30 wt.%, as evidenced by the comparison with the analogous physical mixture.

To verify the effective functionalization of $SiO_2@Al_2O_3$ binary filler with TMSPM silane units, FTIR analysis was preliminary performed (Figure 3). In the case of naked $SiO_2@Al_2O_3$ binary filler, the FTIR analysis reveals the presence of: (i) a broad band at ca. 3500 cm^{-1} due to the presence of hydroxyl functional groups, (ii) a weak signal at ca. 1630 cm^{-1} due to H-O-H scissoring due to traces of physically adsorbed water molecules, (iii) a very intense band centered at ca. 1090 cm^{-1} due to the siloxane asymmetric stretching vibrations of silica, and (iv) a further signal at ca. 600 cm^{-1} due to both Al-O and Si-O bending vibrations.[25,37,49] The effectiveness of the TMSPM functionalization in $SiO_2@Al_2O_3$-TMSPM filler has been confirmed by the presence of the weak signal at ca. 2840 cm^{-1} due to the stretching of TMSPM methylene C-H bonds, and the growth of two signals at ca. 1720 and 1640 cm^{-1}, respectively due to C=O and C=C stretching of TMSPM methacrylic functionalities.[25]

To further assess the binary filler surface functionalization, a ^{13}C CPMAS NMR spectrum was recorded on $SiO_2@Al_2O_3$-TMSPM sample (Figure 4). The analysis supports the conclusions of the FTIR study, in fact all the resonances belonging to the methacryloxypropyl chain are visible.[37,40] In particular, the shift of 1 (Si-CH_2-) up to 10 ppm and the very low intensity of 8 (-OCH_3) indicate an almost complete hydrolysis and condensation of the silane. The C=C double bond (5, 6) is perfectly preserved (Figure 4, left). The related ^{29}Si CPMAS spectrum (Figure 4, right) confirms the presence of the T units onto the binary oxide particles (Q resonance centered at about −100 ppm). The TMSPM is represented by the T^2 and T^3 components at 57 and 66 ppm, respectively.[37,40] It should be mentioned that the CPMAS sequence was chosen to maximize the TMSPM signals, in fact the quantitative MAS NMR spectrum in the present case is useless due to the very low amount of T units with respect to Q.

Finally, to quantitatively estimate the amount of TMSPM functionalizing agent attached on the binary filler surface, TGA was carried out. Table 1 reports the quantification of hydroxyl functionalities at the surface of bare SiO_2 and $SiO_2@Al_2O_3$ binary filler (i.e., necessary for the surface functionalization), and the calculated amount of the TMSPM units at the surface of $SiO_2@Al_2O_3$-TMSPM (see the experimental protocol reported in the Data S1). Results indicate that the amount of -OH groups available at the surface for SiO_2 is one order of magnitude higher than that retrieved for $SiO_2@Al_2O_3$, in accordance with the thermal treatment at 1100°C undergone by the binary filler and necessary for the crystallization of the alumina phase.

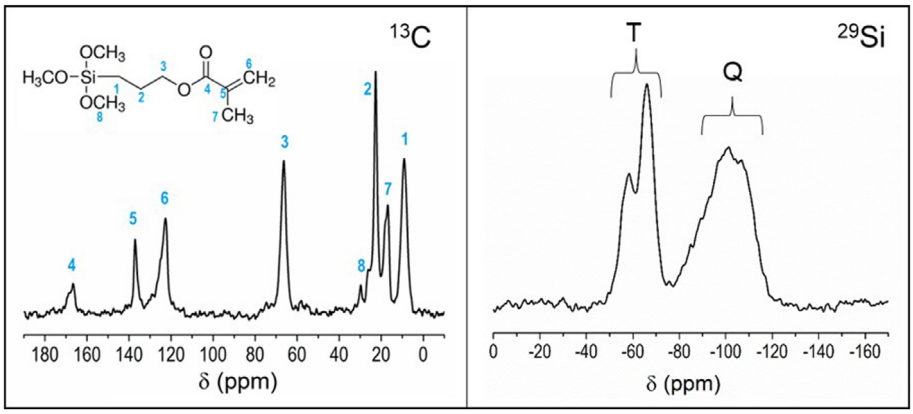

FIGURE 4 ^{13}C and ^{29}Si CPMAS NMR spectra of the SiO_2@Al_2O_3-TMSPM sample.

TABLE 1 Hydroxyl groups and TMSPM units quantifications based on TGA measurements, calculated with the protocol reported in the Data S1.

	Hydroxyl groups quantification		TMSPM units quantification	
Filler	**TGA mass loss (wt.%)**	**n_{OH}/g_{filler} (mol/g)**	**TGA mass loss (wt.%)**	**n_{TMSPM}/g_{filler} (mol/g)**
SiO_2	3.6	$4.46 \cdot 10^{-3}$	-	-
SiO_2@Al_2O_3	0.4	$4.67 \cdot 10^{-4}$	-	-
SiO_2-TMSPM	-	-	7.7	$3.07 \cdot 10^{-4}$
SiO_2@Al_2O_3-TMSPM	-	-	5.2	$4.33 \cdot 10^{-4}$

3.2 | Characterization of the PB/SiO_2@Al_2O_3 nanocomposites

Several attempts were performed for the preparation of PB composites. Percolation threshold was reached for a filler amount of 20 wt.%, while at higher concentrations inhomogeneous materials were obtained. For this reason, the following characterizations were performed exclusively on composites enclosing 20 wt% of filler, that is, PB/20SiO_2-TMSPM, PB/20SiO_2@Al_2O_3, PB/20SiO_2@Al_2O_3-TMSPM, and PB/20SiO_2@Al_2O_3 + TMSPM. The presence of the binary filler in PB/20SiO_2@Al_2O_3-TMSPM nanocomposite was initially assessed by ATR-FTIR analysis (Figure 5), with highlighted the spectral regions of major interest.

Analogous infrared results were obtained in the case of nanocomposites containing both bare SiO_2 and SiO_2@Al_2O_3 (not shown for the sake of brevity). Both Figure 5A and Figure 5B show the main relevant signals due to the PB matrix, namely: =C-H bonds stretching of 3005 cm^{-1}, stretching vibrations of methylene C-H bonds at 2950 and 2940 cm^{-1}, and C=C bonds stretching at 1654 cm^{-1}.[50] At low wavenumbers (Figure 5C), instead, it is possible to register the presence of the intense Si-O stretching band centered at 1090 cm^{-1} due to the inorganic binary filler, which confirms its presence in the nanocomposite.[25]

TGA analyses on nanocomposites were used to experimentally assess the content of inorganic filler, which resulted in agreement with the nominal values (the experimental TGA curves and their relative description are reported in the Data S1).

Furthermore, the filler distribution within the composites has been investigated by means of SEM-EDS analysis. In detail, the micrographs of PB/20SiO_2@Al_2O_3, PB/20SiO_2@Al_2O_3 + TMSPM, and PB/20SiO_2@Al_2O_3-TMSPM were selected as the most significant examples and compared in Figure 6. The images noticeably suggest that surface functionalization exerts a significant influence on the NPs organization in the rubber matrix. In fact, the microanalysis revealed the presence of isolated micrometric aggregates when bare SiO_2@Al_2O_3 fillers are introduced in the PB matrix (Figure 6A). This morphology is explainable considering the lack of compatibility existing between the polar surfaces of the oxide and non-polar polymeric chains of the matrix.

Micrographs indicate the nanocomposites enclosing the binary filler just mixed with the organosilane (PB/20SiO_2@Al_2O_3 + TMSPM, Figure 6B) present a more homogeneous distribution of the particles within the polymeric matrix respect to PB/20SiO_2@Al_2O_3 (Figure 6A). However, still large aggregates are present which appear only partially interconnected across the matrix (Figure 6B). As already observed in our previous studies,[25,37] surface functionalization of SiO_2@Al_2O_3 with the TMSPM seems to favor the filler affinity with the polymer host, favoring the generation of smaller nanometric aggregates homogeneously distributed and probably forming a continuous

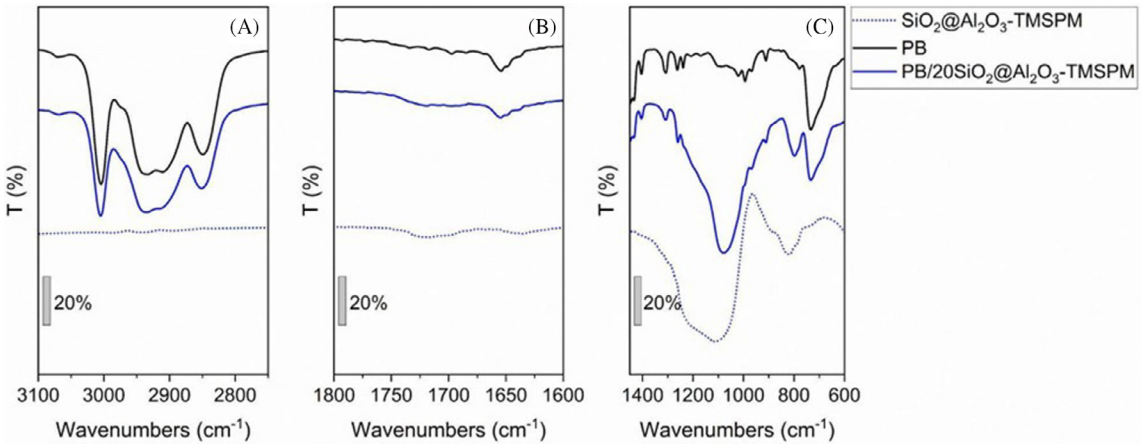

FIGURE 5 ATR-FTIR spectra of bare $SiO_2@Al_2O_3$-TMSPM binary filler (blue dotted line), homopolymerized PB (black dotted line), and $PB/20SiO_2@Al_2O_3$-TMSPM (blue solid line) in the 3100–2750 cm^{-1} range (A), 1800–1600 cm^{-1} (B), and 1450–600 cm^{-1} (C).

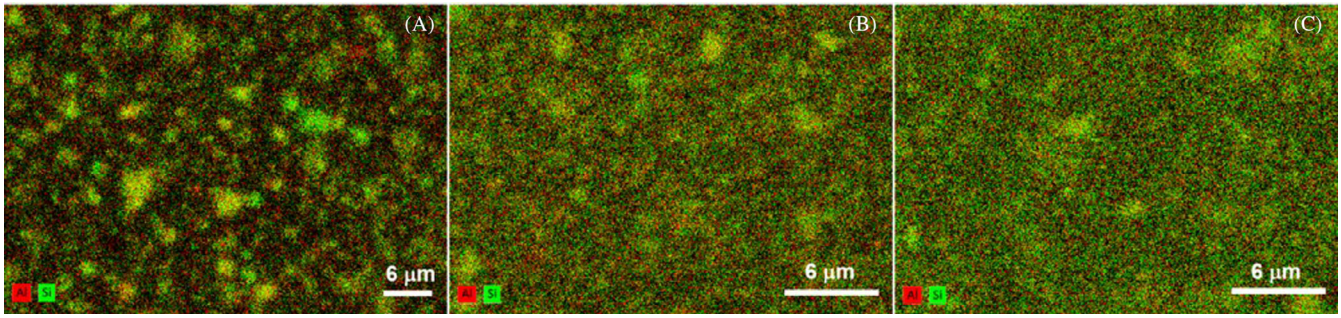

FIGURE 6 SEM-EDS elemental maps of Al and Si of the following nanocomposites: $PB/20SiO_2@Al_2O_3$ (A), $PB/20SiO_2@Al_2O_3$ + TMSPM (B), and $PB/20SiO_2@Al_2O_3$-TMSPM (C) nanocomposites.

filler-filler network (Figure 6C). This peculiar filler arrangement may potentially involve the occurrence of thermally conductive pathways crossing the nanocomposite.

To evaluate the effect of filler incorporation on the structural features of PB matrix ^1H MAS NMR experiments were performed, in particular on the composites enclosing SiO_2-TMSPM, $SiO_2@Al_2O_3$-TMSPM and $SiO_2@Al_2O_3$ + TMSPM. For all the samples the proton spectra of (Figure S5) are dominated by two resonances at both 2.1 and 5.4 ppm, due to PB methylene (=CH_2) and methine (=CH-) functional groups, respectively.[25,38] In detail, a slight narrowing of signal linewidth (LW, i.e., full width at half height) with respect to pure PB can be observed in the nanocomposites, especially in the case of fillers functionalized with TMSPM ($PB/20SiO_2$-TMSPM and $PB/20SiO_2@Al_2O_3$-TMSPM samples), whereas the difference is negligible when the components are just mixed (Figure S5). For elastomers like PB, this effect entails different dynamics at the molecular level induced by the presence of the filler.[25,38] To deepen this aspect, some NMR relaxations experiments were carried out. It is well known that the segmental motion of the long polymeric chains is usually well described by the two processes called spin–spin relaxation and spin–lattice relaxation in the rotating frame (details in the *Experimental* section).[39,40] In both processes, the magnetization (peak intensity) decays with time following exponential laws ruled by two-time constants, T_2 and $T_{1\rho(H)}$, respectively (Figure 7) The time constant values calculated for the analyzed samples from the curves in Figure S6 and Figure S7 are reported in Table S2 (Data S1).

Both relaxation parameters are higher in the composites than in bare PB, indicating an overall polymer stiffening at the molecular level. In particular, the highest $T_{1\rho(H)}$ and T_{2H} values can be obtained for $PB/20SiO_2$-TMSPM, corroborating the marked ability of silica NPs in upgrading the mechanical properties of rubber composites.[30–33]

Interestingly, $PB/20SiO_2@Al_2O_3$-TMSPM displays relaxation times very similar to those calculated for $PB/20SiO_2$-TMSPM and slightly higher compared to the values retrieved for the $SiO_2@Al_2O_3$ + TMSPM mixture. These results, besides indicating that the presence of alumina in the binary filler does not undermine the peculiar capability of silica in providing significant reinforcement,

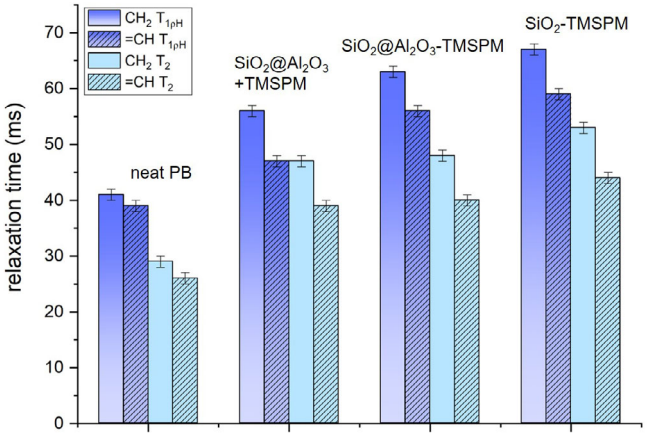

FIGURE 7 Relaxation time constants $T_{1\rho(H)}$ and T_2 obtained from the analysis of the proton spectra and related magnetization curve trends for neat PB and the PB composites enclosing $SiO_2@Al_2O_3$ binary filler mixed with TMSPM (i.e., PB/$SiO_2@Al_2O_3$ + TMSPM sample), $SiO_2@Al_2O3$-TMSPM and SiO_2-TMSPM.

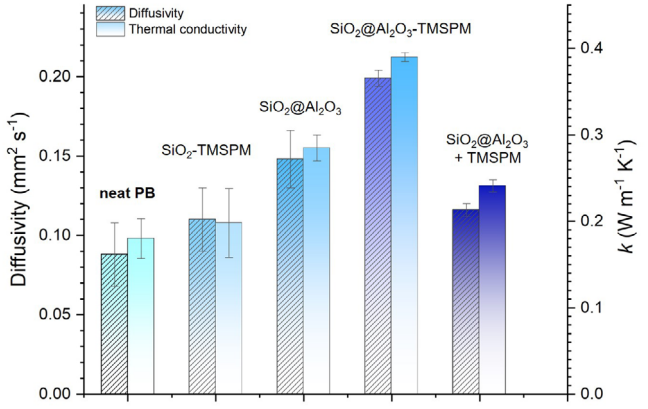

FIGURE 8 Thermal diffusivity and thermal conductivity for the bare PB matrix, and for the composites enclosing SiO_2-TMSPM, $SiO_2@Al_2O_3$, $SiO_2@Al_2O_3$-TMSPM and $SiO_2@Al_2O_3$ binary filler mixed with TMSPM (i.e., PB/$SiO_2@Al_2O_3$ + TMSPM sample).

suggest an effect of the surface functionalization in providing better filler-polymer interaction, which may make easier the thermal transport across the matrix. SEM investigation sounds to support this hypothesis, showing for PB/20$SiO_2@Al_2O_3$-TMSPM the generation of smaller homogeneously distributed nanometric aggregates probably forming a continuous filler-filler network (see Figure 6C).

The thermal transport ability imparted by bare and surface functionalized $SiO_2@Al_2O_3$ binary filler to the rubber composites was assessed by LFA measurements (Figure 8). Data reported are expressed as both diffusivity (which is the "raw measure" of the thermal transport) and thermal conductivity, which was determined according to Equation (1), considering the density of the composites ρ measured by means of He pycnometer and the specific heat capacity C_p obtained by DSC (see Table S3 in Data S1 for details). It is possible to appreciate that the addition of the binary filler generally improves the diffusivity and, in turn, the thermal conductivity of the composites if compared to neat PB or PB/20SiO_2-TMSPM composite. However, only a partial enhancement of the thermal transport can be achieved in the presence of naked $SiO_2@Al_2O_3$ NPs (i.e., PB/20$SiO_2@Al_2O_3$) probably due to the formation of inhomogeneous and large aggregates (as highlighted in Figure 6A), whose scarce interconnections may avoid the generation of thermally conductive pathways. The surface functionalization of the $SiO_2@Al_2O_3$, instead, remarkably upgrades the heat transport capability, with an enhancement of almost 100% of the *k* value with respect to homopolymerized PB and PB/20SiO_2-TMSPM. This unique effect becomes much more evident when compared to the performance of PB/20$SiO_2@Al_2O_3$ + TMSPM, obtained by physically mixing bare $SiO_2@Al_2O_3$ and neat TMSPM, which result remarkably lower and similar to those of the composite enclosing functionalized silica NPs (Figure 8).

These results can be rationalized considering the SEM images of PB/20$SiO_2@Al_2O_3$-TMSPM sample (Figure 6C), where it is registered the formation of micrometric and/or sub-micrometric filler aggregates homogeneously distributed inside the polymer host and partially interconnected, which may reduce interfacial thermal resistance phenomena providing efficient thermal conductive pathways. On the other hand, when the silane is just mixed with $SiO_2@Al_2O_3$ (i.e., PB/20$SiO_2@Al_2O_3$ + TMSPM sample), it most likely binds to the silica surface rather than to alumina nanosheets or, possibly, it may undergo self-condensation, thus leading to generation of isolated aggregates inhibiting the thermal transport (see Figure 6B).

NMR proton relaxation behavior in PB/20$SiO_2@Al_2O_3$-TMSPM supports at the molecular level these considerations, underlining the role of the surface functionalization in promoting the stiffening of the polymer chains, as a result of improved filler-polymer interaction which may foster the thermal transport across the matrix.

To sum up, not only the alumina growth on the silica surface provides an improvement of the thermal conductivity, but also the functionalization seems to play a role, mitigating the filler-rubber interfacial thermal resistance.

4 | CONCLUSIONS

With the aim to synergistically combine the intrinsic thermal conductivity properties of Al_2O_3 with the peculiar reinforcement ability of silica in rubber composites, a

new binary filler system, $SiO_2@Al_2O_3$, was developed by an easy, scalable and water-based soft-chemistry strategy.

The in depth structural and morphological characterizations revealed that the material is constituted by γ-alumina crystalline nanosheets grown at the surface of amorphous SiO_2 nanoparticles aggregates. The binary filler was used naked or suitably surface functionalized with TMSPM to prepare cis-polybutadiene model composites by a simple solvent casting technique.

SEM-EDS investigation and solid-state NMR unveiled that the presence of alumina in the binary filler does not undermine the capability of silica in generating polymer chains stiffening and, thus, in delivering reinforcement. Moreover, they suggested a significant effect of the surface silanization in providing a trade-off between filler networking and interaction with the PB matrix which, in principle, may reduce interfacial thermal resistance and facilitate the thermal transport.

Accordingly, the thermal conductivity measurements highlighted that the introduction of the $SiO_2@Al_2O_3$ binary filler in PB induces a remarkable upgrade of the heat transport capability, especially upon surface modification with TMSPM, with an enhancement of almost 100% of the *k* value with respect to homopolymerized PB and of about 80% compared to the composite obtained by physically mixing bare $SiO_2@Al_2O_3$ and neat TMSPM.

In summary, the results of the present study appear promising, since they provide a way to introduce with a relatively cheap and green methodology thermally conductive alumina in rubber composites, notwithstanding its different chemistry compared to common silica filler, thus envisaging a possible large-scale application of $SiO_2@Al_2O_3$ in tires tread formulations.

AUTHOR CONTRIBUTIONS

Lorenzo Mirizzi: Data curation, Formal analysis, Writing—review & editing. **Andreia Amighini Alerhush**: Data curation, Formal analysis, Writing—review & editing. **Roberto Nisticò**: Data curation, Methodology, Writing—original draft, Writing—review & editing. **Mery Malandrino**: Data curation, Formal analysis, Writing—review & editing. **Sandra Diré**: Data curation, Formal analysis, Writing—review & editing. **Emanuela Callone**: Data curation, Formal analysis, Writing—review & editing. **Giulia Fredi**: Data curation, Formal analysis, Writing—review & editing. **Andrea Dorigato**: Data curation, Formal analysis, Writing—review & editing. **Luca Giannini**: Methodology, Writing—review & editing. **Silvia Guerra**: Methodology, Writing—review & editing. **Silvia Mostoni**: Formal analysis, Methodology, Writing—review & editing. **Barbara Di Credico**: Methodology, Writing—review & editing. **Roberto Scotti**: Methodology, Writing—review & editing. **Massimiliano D'Arienzo**: Conceptualization, Data curation, Methodology, Writing—original draft, Writing—review & editing.

ACKNOWLEDGMENTS

L.M. thanks CORIMAV (Consortium for the Research of Advanced Materials between Pirelli and Milano Bicocca University) for its support within the PCAM European Doctoral Program.

CONFLICT OF INTEREST STATEMENT

The authors declare no conflict of interest.

DATA AVAILABILITY STATEMENT

Data will be made available on request.

ORCID

Roberto Nisticò https://orcid.org/0000-0001-8986-5542
Giulia Fredi https://orcid.org/0000-0001-9987-1786

REFERENCES

1. Ishikawa T, Amaoka K, Masubuchi Y, et al. Overview of automotive structural composites technology developments in Japan. *Compos Sci Technol*. 2018;155:221-246. doi:10.1016/j.compscitech.2017.09.015
2. Khan A, Kian LK, Jawaid M, et al. Preparation and characterization of lignin/nano graphene oxide/styrene butadiene rubber composite for automobile tyre application. *Int J Biol Macromol*. 2022;206:363-370. doi:10.1016/j.ijbiomac.2022.02.146
3. Hu H. Recent advances of polymeric phase change composites for flexible electronics and thermal energy storage system. *Compos Part B Eng*. 2020;195:108094. doi:10.1016/j.compositesb.2020.108094
4. Tan P, Wang H, Xiao F, et al. Solution-processable, soft, self-adhesive, and conductive polymer composites for soft electronics. *Nat Commun*. 2022;13:358. doi:10.1038/s41467-022-28027-y
5. Scardaci V, Rozhin AG, Hennrich F, Milne WI, Ferrari AC. Carbon nanotube-polymer composites for photonic devices. *Physica E Low Dimens Syst Nanostruct*. 2007;37:115-118. doi:10.1016/j.physe.2006.08.001
6. Ramakrishna S, Mayer J, Wintermantel E, Leong KW. Biomedical applications of polymer-composite materials: a review. *Compos Sci Technol*. 2001;61:1189-1224. doi:10.1016/S0266-3538(00)00241-4
7. Rezwan K, Chen QZ, Blaker JJ, Boccaccini AR. Biodegradable and bioactive porous polymer/inorganic composite scaffolds for bone tissue engineering. *Biomaterials*. 2006;27:3413-3431. doi:10.1016/j.biomaterials.2006.01.039
8. Zhang M, Biesold GM, Choi W, et al. Recent advances in polymers and polymer composites for food packaging. *Mater Today*. 2022;53:134-161. doi:10.1016/j.mattod.2022.01.022
9. Guo Y, Ruan K, Shi X, Yang X, Gu J. Factors affecting thermal conductivities of the polymers and polymer composites: a review. *Compos Sci Technol*. 2020;193:108134. doi:10.1016/j.compscitech.2020.108134

10. Nisticò R, D'Arienzo M, Di Credico B, Mostoni S, Scotti R. The role of inorganic fillers in electrostatic discharge composites. *Inorganics*. 2022;10:222. doi:10.3390/inorganics10120222
11. Xu Y, Wang X, Hao Q. A mini review on thermally conductive polymers and polymer-based composites. *Compos Commun*. 2021;24:100617. doi:10.1016/j.coco.2020.100617
12. Yu X, Bhatti MR, Ren X, et al. Dieletric polymer composites with ultra-high thermal conductivity and low dielectric loss. *Compos Sci Technol*. 2022;229:109695. doi:10.1016/j.compscitech.2022.109695
13. Danilova-Tretyak SM. On thermophysical properties of rubbers and their components. *J Eng Phys Thermophys*. 2016;89:1388-1393. doi:10.1007/s10891-016-1506-5
14. Nisticò R, Lavagna L, Boot EA, et al. Improving rubber concrete strength and toughness by plasma-induced end-of-life tire rubber surface modification. *Plasma Process Polym*. 2021;18:e2100081. doi:10.1002/ppap.202100081
15. Sokolov SL. Analysis of the heat state of pneumatic tires by the finite element method. *J Mach Manuf Reliab*. 2009;38:310-314. doi:10.3103/S1052618809030182
16. Wang Z, Lu Y, Ding J, Zhang L, Chan TW. Preparation of nano-reinforced thermal conductive natural rubber composites. *Polym Compos*. 2016;37:771-781. doi:10.1002/pc.23234
17. Mirizzi L, Carnevale M, D'Arienzo M, et al. Tailoring the thermal conductivity of rubber nanocomposites by inorganic systems: opportunities and challenges for their application in tires formulation. *Molecules*. 2021;26:3555. doi:10.3390/molecules26123555
18. EU. Regulation (EU) 2020/740 of the European Parliament and of the council of 25 may 2020 on the labelling of tyres with respect to fuel efficiency and other parameters, amending regulation (EU) 2017/1369 and repealing regulation (EC) No 1222/2009. *Off J Eur Union*. 2019;2019(1919):20-21.
19. Danafar F, Kalantari M. A review of natural rubber nanocomposites based on carbon nanotubes. *J Rubber Res*. 2018;21:293-310. doi:10.1007/BF03449176
20. Han Z, Fina A. Thermal conductivity of carbon nanotubes and their polymer nanocomposites: a review. *Prog Polym Sci*. 2011;36:914-944. doi:10.1016/j.progpolymsci.2010.11.004
21. Ate S, Subramaniam C, Nashizawa A, Yamada T, Hata K. Highly thermally conductive yet flexible composite of carbon fiber, carbon nanotube, and rubber obtained by decreasing the thermal resistivity at the interface between carbon fiber and carbon nanotube. *Adv Eng Mater*. 2007;19:1600596. doi:10.1002/adem.201600596
22. Song SH, Kim JM, Park KH, et al. High performance graphene embedded rubber composites. *RSC Adv*. 2015;5:81707-81712. doi:10.1039/C5RA16446J
23. Yin B, Wang J, Jia H, He J, Zhang X, Xu Z. Enhanced mechanical properties and thermal conductivity of styrene–butadiene rubber reinforced with polyvinylpyrrolidone-modified graphene oxide. *J Mater Sci*. 2016;51:5724-5737. doi:10.1007/s10853-016-9874-y
24. Yang H, Cai F, Luo Y, Ye X, Zheng C, Wu S. The interphase and thermal conductivity of graphene oxide/butadiene-styrene-vinyl pyridine rubber composites: a combined molecular simulation and experimental study. *Compos Sci Technol*. 2020;188:107971. doi:10.1016/j.compscitech.2019.107971
25. Mirizzi L, D'Arienzo M, Nisticò R, et al. Al_2O_3 decorated with POSS units: an unconventional filler system for upgrading thermal conductivity and mechanical properties of rubber composites. *Compos Sci Technol*. 2023;236:109977. doi:10.1016/j.compscitech.2023.109977
26. Fang H, Bai S-L, Wong CP. "White graphene"—hexagonal boron nitride based polymeric composites and their application in thermal management. *Compos Commun*. 2016;2:19-24. doi:10.1016/j.coco.2016.10.002
27. Jiang C, Zhang D, Gan X, Xie R, Zhang F, Zhou K. Preparation of high performance AlN/hydantion composite by gelcasting and infiltration processes. *Ceram Int*. 2014;40:2535-2538. doi:10.1016/j.ceramint.2013.07.131
28. Shen D, Zhan Z, Liu Z, et al. Enhanced thermal conductivity of epoxy composites filled with silicon carbide nanowires. *Sci Rep*. 2017;7:2606. doi:10.1038/s41598-017-02929-0
29. Mu Q, Feng S, Diao G. Thermal conductivity of silicone rubber filled with ZnO. *Polym Compos*. 2007;28:125-130. doi:10.1002/pc.20276
30. Uhrlandt S, Blume A. Silica in green tyres-processes, products, properties. *Kautschuk Gummi Kunststoffe*. 2001;54:520.
31. Scotti R, Conzatti L, D'Arienzo M, et al. Shape controlled spherical (0D) and rod-like (1D) silica nanoparticles in silica/styrene butadiene rubber nanocomposites: role of the particle morphology on the filler reinforcing effect. *Polymer*. 2014;55:1497-1506. doi:10.1016/j.polymer.2014.01.025
32. Di Credico B, Cobani E, Callone E, et al. Size-controlled self-assembly of anisotropic sepiolite fibers in rubber nanocomposites. *Appl Clay Sci*. 2018;152:51-64. doi:10.1016/j.clay.2017.10.032
33. Tadiello L, D'Arienzo M, Di Credico B, et al. The filler-rubber interface in styrene butadiene nanocomposites with anisotropic silica particles: morphology and dynamic properties. *Soft Matter*. 2015;11:4022-4033. doi:10.1039/c5sm00536a
34. Wang Z-H, Lu Y-L, Liu J, Dang Z-M, Zhang L-Q, Wang W. Preparation of nanoalumina/EPDM composites with good performance in thermal conductivity and mechanical properties. *Polym Adv Technol*. 2011;22:2302-2310. doi:10.1002/pat.1761
35. Vaisakh SS, Mohammed AAP, Hassanzadeh M, Tortorici JF, Metz R, Ananthakumar S. Effect of nano-modified SiO_2/Al_2O_3 mixed-matrix micro-composite fillers on thermal, mechanical, and tribological properties of epoxy polymers. *Polym Adv Technol*. 2016;27:905-914. doi:10.1002/pat.3747
36. Roh H-S, Choi CK, An J-S, et al. Size-controlled synthesis of monodispersed mesoporous α-alumina spheres by a template-free forced hydrolysis method. *Dalton Trans*. 2011;40:6901-6905. doi:10.1039/C1DT10418G
37. D'Arienzo M, Diré S, Cobani E, et al. SiO_2/ladder-like polysilsesquioxanes nanocomposite coatings: playing with the hybrid interface for tuning thermal properties and wettability. *Coatings*. 2020;10:913. doi:10.3390/coatings10100913
38. D'Arienzo M, Diré S, Masneri V, et al. Tailoring the dielectric and mechanical properties of polybutadiene nanocomposites by using designed ladder-like polysilsesquioxanes. *ACS Appl Nano Mater*. 2018;1:3817-3828. doi:10.1021/acsanm.8b00558
39. Dreiss CA, Cosgrove T, Benton NJ, et al. Effect of crosslinking on the mobility of PDMS filled with polysilicate nanoparticles: positron lifetime, rheology and NMR relaxation studies. *Polymer*. 2007;48:4419-4428. doi:10.1016/j.polymer.2007.05.070
40. Dirè S, Callone E, Ceccato R, et al. Structural effects of TiO_2 nanoparticles in photocurable ladder-like polysilsesquioxane

nanocomposites. *J Sol-Gel Sci Technol*. 2023. doi:10.1007/s10971-023-06127-5

41. Nisticò R, Magnacca G, Antonietti M, Fechler N. "Salted silica": sol-gel chemistry of silica under hypersaline conditions. *Z Anorg Allg Chem*. 2014;640:582-587. doi:10.1002/zaac.201300526
42. Smith SJ, Amin S, Woodfield BF, Boerio-Goates J, Campbell BJ. Phase progression of γ-Al_2O_3 nanoparticles synthesized in a solvent-deficient environment. *Inorg Chem*. 2013;52:4411-4423. doi:10.1021/ic302593f
43. Jbara AS, Othaman Z, Ati AA, Saeed MA. Characterization of γ-Al_2O_3 nanopowders synthesized by co-precipitation method. *Mater Chem Phys*. 2017;188:24-29. doi:10.1016/j.matchemphys.2016.12.015
44. Rashidi F, Kharat AN, Rashidi AM, Lima E, Lara V, Valente JS. Fractal geometry approach to describe mesostructured boehmite and gamma-alumina nanorods. *Eur J Inorg Chem*. 2010;2010:1544-1551. doi:10.1002/ejic.200901103
45. Greiser S, Gluth GJG, Sturm P, Jager C. $^{29}Si\{^{27}Al\}$, $^{27}Al\{^{29}Si\}$ and $^{27}Al\{^{1}H\}$ double-resonance NMR spectroscopy study of cementitious sodium aluminosilicate gels (geopolymers) and gel–zeolite composites. *RSC Adv*. 2018;8:40164-40171. doi:10.1039/C8RA09246J
46. Hiet J, Deschamps M, Pellerin N, Fayon F, Massiot D. Probing chemical disorder in glasses using silicon-29 NMR spectral editing. *Phys Chem Chem Phys*. 2009;11:6935-6940. doi:10.1039/B906399D
47. Fedel M, Callone E, Diré S, Deflorian F, Olivier M-G, Poelman M. Effect of Na-montmorillonite sonication on the protective properties of hybrid silica coatings. *Electrochim Acta*. 2014;124:90-99. doi:10.1016/j.electacta.2013.11.006
48. Takahashi T, Ohkubo T, Suzuki K, Ikeda Y. High resolution solid-state NMR studies on dissolution and alteration of Na-montmorillonite under highly alkaline conditions. *Microporous Mesoporous Mater*. 2007;106:284-297. doi:10.1016/j.micromeso.2007.03.008
49. D'Arienzo M, Redaelli M, Callone E, et al. Hybrid SiO_2@POSS nanofiller: a promising reinforcing system for rubber nanocomposites. *Mater Chem Front*. 2017;1:1441-1452. doi:10.1039/C7QM00045F
50. Liu X, Zhou T, Liu Y, Zhang A, Yuan C, Zhang W. Cross-linking process of cis-polybutadiene rubber with peroxides studied by two-dimensional infrared correlation spectroscopy: a detailed tracking. *RSC Adv*. 2015;5:10231-10242. doi:10.1039/C4RA13502D

SUPPORTING INFORMATION

Additional supporting information can be found online in the Supporting Information section at the end of this article.

How to cite this article: Mirizzi L, Amighini Alerhush A, Nisticò R, et al. SiO_2@Al_2O_3 binary filler: A chance for enhancing the heat transport in rubber composites for tire applications. *Polym Compos*. 2024;1-13. doi:10.1002/pc.28326